

Finite Element Modelling of Penetration Tests into Martian analogue Materials

27 June – 1 July 2005, Anavyssos, Attica, Greece

A. Zöhrer⁽¹⁾, G. Kargl⁽²⁾

⁽¹⁾ Space Research Institute, Austrian Academy of Sciences, Schmiedlstrass 6, 8042 Graz, Austria,
Email: alexander.zoehrer@oeaw.ac.at

⁽²⁾ Space Research Institute, Austrian Academy of Sciences, Schmiedlstrass 6, 8042 Graz, Austria,
Email: guenter.kargl@oeaw.ac.at

ABSTRACT

The development of a numerical model to simulate the penetration of a probe into regolith materials is the main part of our work. In particular we deal with small-scale penetration instruments which can be implemented on Martian landers.

For the numerical simulation the programme ABAQUS/Standard, which is based on the finite element method, is used. It offers the possibility to model the frictional surfaces between the probe and the sample and can handle the large relative displacements. Further a remeshing algorithm can be implemented as well as user defined soil models. In addition to the numerical modelling some results of the laboratory work are presented within this paper.

1. INTRODUCTION

The planet Mars is one of the most attractive targets for space missions in the present and the next decades. Even though the planet is already quite well mapped from the orbit, in situ exploration on the surface is much less advanced. In the face of the human Martian exploration programme, which is planned and scheduled for the next 30 years, the design of large habitats and vehicles will be necessary. Therefore the knowledge of the main soil mechanical parameters of the Martian soils is required.

Up to now there exists only little information about the composition of the Martian soils. A geological investigation can be done with remote methods using techniques from the field of geophysics at a sufficient level of accuracy, but only an in situ exploration can determine reliable mechanical parameters.

Because of its small and light weighted construction type, the Cone Penetration Test is a useful investigation method for space missions though in smaller scale than in geotechnical

practice. The probe itself can also be integrated into other instruments of a landing probe, as it was realized e.g. for the Rosetta lander [1,2].

With our penetration test stand we can investigate different Martian analogue materials with tip shapes similar to flight-ready probes. In addition to the presentation of the laboratory work the main focus of this paper will be on the development of a numerical model to simulate the penetration progress. For the simulation the Finite Element Method (FEM) is used.

2. MARTIAN ANALOGUE MATERIALS

The first step was to find materials that are suitable for the penetration tests and which come close to the actual Martian soil with regard to geotechnical parameters. For that reason several points were taken into account for the selection of the materials. As a result of former missions there are estimated parameters for the surface material of Mars [3]. Based on this data several Martian analogue materials were selected. Because the availability of these analogue materials is quite limited, similar local materials were chosen. The range of the used materials concerning the grain size is from fine silt to coarse sand.

The two selected Martian analogue materials are the Salten Skov iron precipitate from Denmark and the JSC-Mars 1 from Johnson Space Centre (Hawaii), which were both available only in limited amounts. In addition to the Martian analogue materials local materials were selected. These are two silty sands called Schwarzl UK4 and Fohnsdorfer Haldit that are similar to the analogue materials.

Fig. 1 shows the particle size distribution curves of all four materials. You can see the correlation between the JSC Mars-1 and the Schwarzl UK4 and the correlation between the Salten Skov and the Fohnsdorfer Haldit.

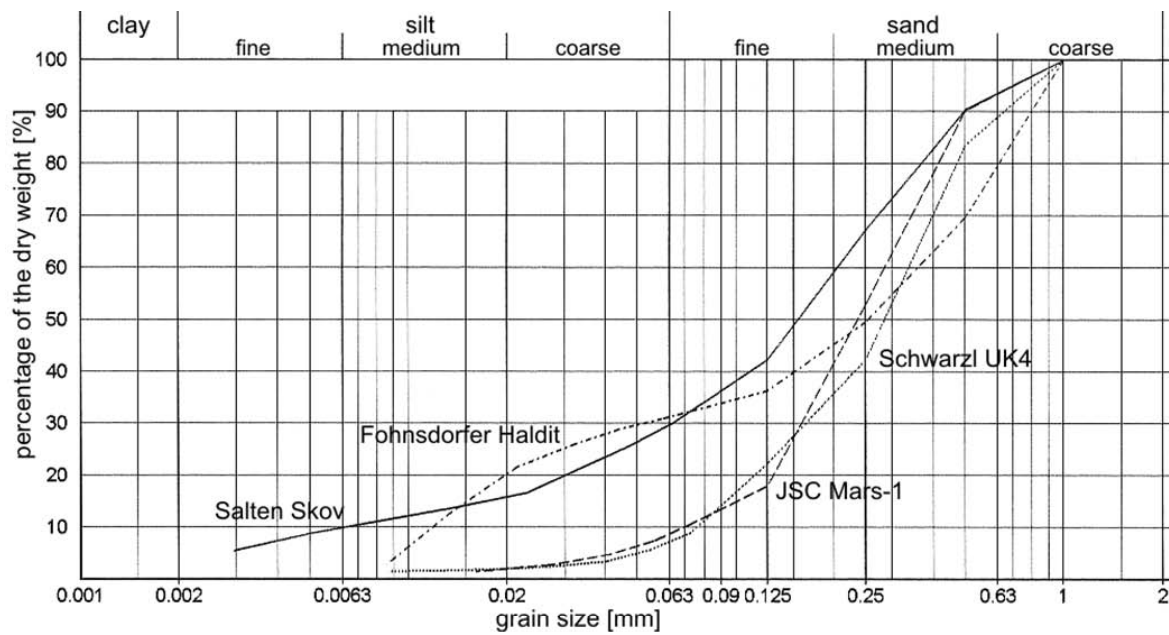


Fig. 1: Particle size distribution curves of the four selected materials

3. PENETRATION TESTS IN THE LABORATORY

3.1 Principle of penetration testing

During the test a conical tip (Fig. 2) is pushed into the ground at a constant rate, while the reaction force to the tip and the sleeve friction is measured continuously. The rate of penetration is quite slow, so any dynamic influences can be neglected. The geometry of the probe in Fig. 2 refers to the reference test equipment which is standardised worldwide.

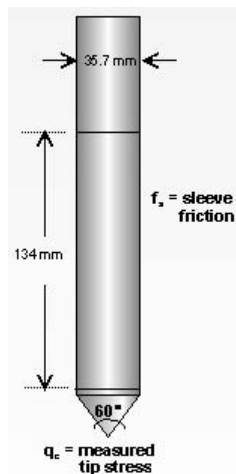


Fig 2: reference cone

In geotechnical practice this procedure is called cone penetration test (CPT) and is a quite common test to investigate the ground strata and to drive the strength and compressibility of primarily cohesionless soils. The principle of the evaluation of CPT is to get correlations between the reaction forces to the tip and different soil mechanical parameters. After reaching a certain depth the tip resistance is mainly influenced by the properties of the soil and not by the overburden pressure. So it is possible to correlate the tip resistance directly to geotechnical parameters.

Due to the fact that CPT is used commonly since the 1980s, a large number of diagrams to evaluate the measured forces for different soil types exists. Further details on CPT in geotechnical practice are given in [4].

The main difference between the CPT in the field of geotechnics on earth and the penetration tests performed on Martian landers is the penetration depth. CPTs can reach depths of 50 m, while the penetration depth of an instrument implemented on a lander is limited to less than one meter. In our case we investigate only the uppermost layer of the surface, so the penetration depth in our laboratory tests as well as for the numerical simulation is about 20 cm. This is why we can not assign a typical tip force which is independent of the depth, to a set of geotechnical parameters. Now we have to take the penetration depth as well as the distribution of the tip force over the depth into account.

3.2 Laboratory tests

The principal test set-up for the laboratory penetration tests is shown in Fig. 3. There are usually two sensors integrated into the penetrating rod. One sensor is placed right behind the tip referred to as “Test sensor” and the second is located about 20 cm above (“Monitor sensor”). Both sensors have a nominal load of 500 N, however they can be replaced by sensors with nominal loads of 25 N and 100 N, respectively.

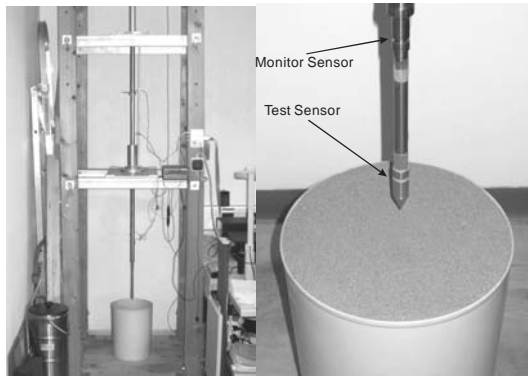


Fig. 3: Penetration test set-up

The conical tip which is shown in Fig. 3 has an opening angle of 45° and a diameter of 1,8 cm. The maximum depth reached with this test set-up is 21 cm. The sample is filled into an approximately cylindrical container which is 33,3 cm high and has an upper rim diameter of 26,2 cm. Thus, on the one hand the container is large enough, that boundary effects hardly influence the results and on the other hand the required amount of material is kept in a practical magnitude.

In addition to the tip mentioned above four more tip shapes (Fig. 4) are used in different test series. The tips have opening angles of 30° , 45° and 60° , plus a spherical and a flat tip.

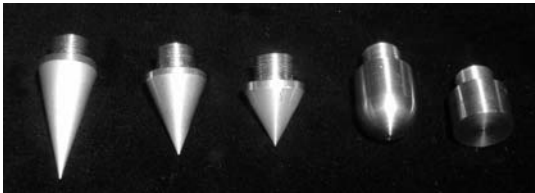


Fig. 4: different tip shapes

A very important part of penetration test into sandy materials is the preparation of the sample. To get valuable and reproducible results the material has to be homogenous and with the same density from bottom to top. In the series of tests presented here the initial dry densities varied from $1,35 \text{ g/cm}^3$ to $1,55 \text{ g/cm}^3$ which corresponds to a loose to medium dense package.

To achieve this known and homogenous package the material is filled into the container in several layers. All layers are of the same thickness and are compressed with the same energy. The sample surface coincides with the upper edge of the sample container. The advantage of this is that the sample surface is completely flat and so the volume can be determined with high precision. The total mass of the material in the container is measured and so the density can be calculated.

The next figure (Fig. 5) illustrates the difference of the measured forces by the test- and the monitor sensor. For the upper approx. 10 cm the measured values are almost the same. Beneath this depth the influence of the sleeve friction increases the value of the monitor sensor compared to the test sensor. Because the diameter of the rod is smaller than the diameter of the tip, the force caused by sleeve friction is only about 10 % of the maximum tip force.

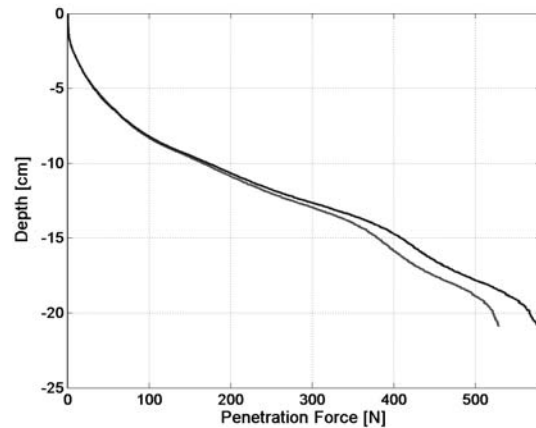


Fig. 5: Penetration forces ($\rho_d = 1,55 \text{ g/cm}^3$)

Fig. 6 shows the results of three tests with different initial densities, varying from loose to medium dense. While the maximum penetration force reached is only about 30 N for the loosest package, it increases to more than 500 N for the test with an initial dry density of $1,55 \text{ g/cm}^3$.

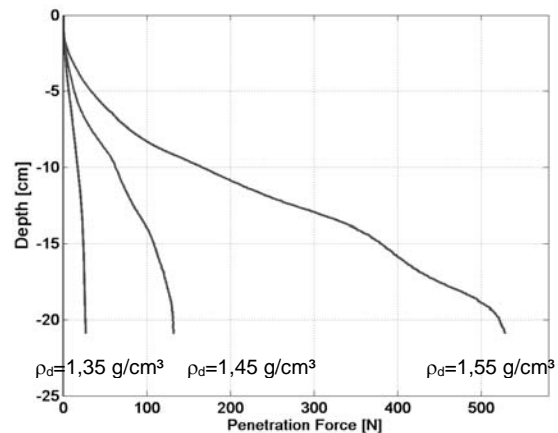


Fig. 6: Comparison of three tests

4. NUMERICAL SIMULATION

To evaluate the results received from instruments on planet Mars we are faced with different boundary conditions that can not be considered correctly in a laboratory test as for example the gravity. Therefore, it is necessary to have a comparison matrix with previously investigated materials. So it is unavoidable to use a numerical programme with a previously calibrated soil model to predict realistic results for penetration tests under Martian conditions.

As an additional advantage of a numerical model the large number of laboratory tests for parametric studies can be reduced. The information derived from the geotechnical tests as well as from the laboratory penetration tests are used to calibrate the numerical calculation.

Even though the geometry of the test is simple, the numerical modelling with the finite element method of the penetration test is quite demanding for the used software. Due to the large relative displacements between the surface of the cone and the surrounding soil it is necessary to separate the discretization of these two parts and reconnect them using a contact interface. Another problem is the severe distortion of elements near and below the tip of the cone. Using finer meshes leads to numerical instabilities that can only be handled by a remeshing algorithm. Furthermore the used software should offer the possibility to use high sophisticated material models.

For the numerical modelling different programmes were tested. Here we report on the work with the software ABAQUS 6.5, which satisfies the special requirements listed above and so this software was already used for related tasks [5,6].

4.1 Preliminaries on Material Modelling

The mechanical behaviour of soils may be modelled at various degrees of accuracy. Hook's law of linear, isotropic elasticity, for example, may be thought of as the simplest available stress-strain relationship. As it involves only two input parameters, Young's modulus and Poisson's ratio, it is generally too crude to capture essential features of soil behaviour. However, for modelling structural elements, e.g. the penetrating cone, linear elasticity tends to be an appropriate approach.

Generally a material model is a set of mathematical equations that describe the relationship between stress and strain. Material models are often expressed in a form in which infinitesimal increments of strains (or 'strain rates') are related to infinitesimal increments of stress (or 'stress rates').

4.1.1 General definitions of stress

Stress is a tensor which can be represented by a matrix in Cartesian coordinates:

$$\underline{\underline{\sigma}} = \begin{bmatrix} \sigma_{xx} & \sigma_{xy} & \sigma_{xz} \\ \sigma_{yx} & \sigma_{yy} & \sigma_{yz} \\ \sigma_{zx} & \sigma_{zy} & \sigma_{zz} \end{bmatrix} \quad (1)$$

In the standard deformation theory, the stress tensor is symmetric such as $\sigma_{xy} = \sigma_{yx}$, $\sigma_{yz} = \sigma_{zy}$, $\sigma_{xz} = \sigma_{zx}$. In this situation, stresses are often written in vector notation, which involve only six different components:

$$\underline{\sigma} = (\sigma_{xx} \quad \sigma_{yy} \quad \sigma_{zz} \quad \sigma_{xy} \quad \sigma_{yz} \quad \sigma_{zx})^T \quad (2)$$

According to Terzaghi's principle, stresses are divided into effective stresses σ' and pore pressures σ_w .

$$\underline{\sigma} = \underline{\sigma}' + \underline{\sigma}_w \quad (3)$$

In our case, we use only dry samples, so that the pore pressures σ_w are equal to zero and thus the stresses σ are equal to the effective stresses σ' . Positive stress components are considered to represent tension, whereas negative stress components indicate pressure (or compression). It is often useful to use principle stresses ($\sigma_1, \sigma_2, \sigma_3$) rather than Cartesian stress components when formulating material models. Principal stresses are the stresses in such a coordinate system direction that all shear stress components are zero. Principal stresses are, in fact, the eigenvalues of the stress tensor. σ_1 is the largest compressive principle stress and σ_3 the smallest.

4.1.2 General definitions of strain

Strain is a tensor which can be represented by a matrix with Cartesian coordinates as:

$$\underline{\underline{\varepsilon}} = \begin{bmatrix} \varepsilon_{xx} & \varepsilon_{xy} & \varepsilon_{xz} \\ \varepsilon_{yx} & \varepsilon_{yy} & \varepsilon_{yz} \\ \varepsilon_{zx} & \varepsilon_{zy} & \varepsilon_{zz} \end{bmatrix} \quad (4)$$

According to the small deformation theory, only the sum of complementing Cartesian shear strain

components ε_{ij} and ε_{ji} result in shear stress. This sum is denoted as shear strain γ . Hence, instead of $\varepsilon_{xy}, \varepsilon_{yx}, \varepsilon_{yz}, \varepsilon_{zy}, \varepsilon_{xz}, \varepsilon_{zx}$ the shear strain components $\gamma_{xy}, \gamma_{yz}, \gamma_{zx}$ are used respectively. Under the above conditions, strains are often written in vector notations, which involve only six different components:

$$\underline{\varepsilon} = (\varepsilon_{xx} \quad \varepsilon_{yy} \quad \varepsilon_{zz} \quad \gamma_{xy} \quad \gamma_{yz} \quad \gamma_{zx})^T \quad (5)$$

Similar as for stresses, positive normal strain components refer to extension, whereas negative normal stress components indicate compression. A strain invariant that is often used is the volumetric strain ε_v , which is defined as the sum of all normal strain components:

$$\varepsilon_v = \varepsilon_{xx} + \varepsilon_{yy} + \varepsilon_{zz} = \varepsilon_1 + \varepsilon_2 + \varepsilon_3 \quad (6)$$

The volumetric strain is defined as negative for compaction and as positive for dilatancy.

4.1.3 Drucker-Prager Model

The sample behaviour is modelled with an extended Drucker-Prager constitutive model. This model is used for frictional materials, which are typically granular-like soils and rocks. It exhibits pressure-dependent yield which means that the material becomes stronger as the pressure increases. The yield criteria for the Drucker-Prager models are based on the shape of the yield surface in the meridional plane (π -plane). In ABAQUS/Standard the yield surface can have a linear form, a hyperbolic form or a general exponent form. The surface for the linear model, which was mainly used for the calculation is illustrated in Fig. 7.

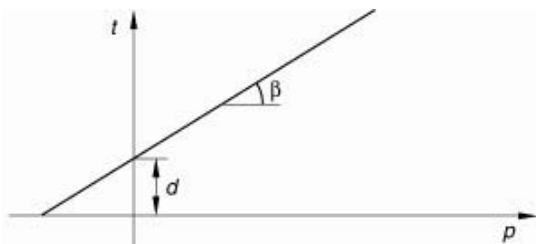


Fig. 7: linear Drucker-Prager model

The linear model provides for a possibly noncircular yield surface in the deviatoric plane to match different yield values in triaxial tension and compression, associated inelastic flow in the deviatoric plane, and separate dilation and friction angles. A more detailed description of the constitutive law can be found in [7].

4.2 Description of the model

The geometry of the axisymmetric numerical model is illustrated in Fig. 8. The sample has the same dimensions as the tub used for the laboratory tests and it is discretised with a FE mesh consisting of 1200 quadrilateral elements. The size of the elements decreases near to the region where the cone penetrates into the sample to achieve a higher accuracy. The cone itself is modelled as a rigid body because the stiffness of the cone is about 10^4 times the stiffness of the soil and so the deformation of the cone can be neglected.

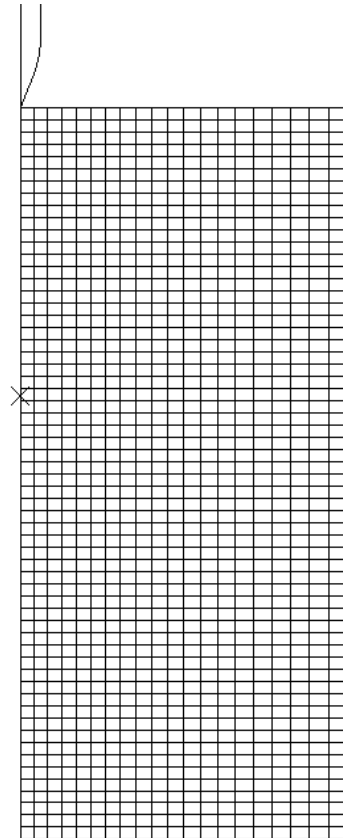


Fig. 8: FE mesh with 1200 quad elements

4.2.1 Calculation procedure

The calculation consists of two steps: In the first step the gravity load is applied to the sample and the initial stress state is calculated.

In the second step the rigid probe penetrates the sample at a constant rate which is similar to the one from the laboratory tests. Because the nodes on the left boundary of the sample must not be fixed to the axis of symmetry there is a frictionless pipe with a very small diameter of 0.1 mm around the axis. So the tip of the penetrometer can penetrate into this pipe and displace the nodes from the

surface of the pipe. In Fig. 9 the upper left part of the model is shown before and shortly after the start of the simulation.

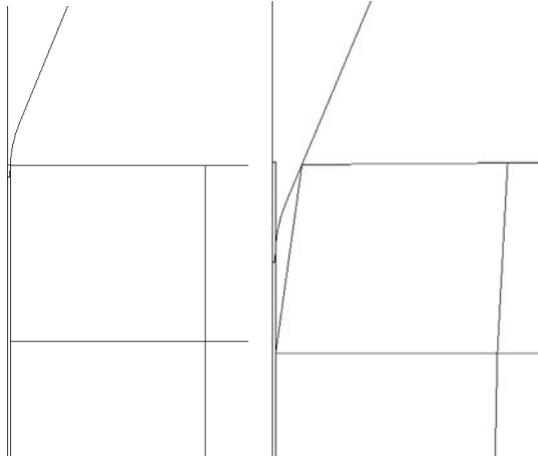


Fig. 9: left boundary of the model

The contact between the sample and the penetrometer is modelled with a surface-to-surface contact. By defining the contact interaction properties the normal (hard contact) and the tangential behaviour (coefficient of friction) can be defined. With this method it is possible to handle the large relative displacements between the cone and the sample.

4.2.2 Adaptive mesh algorithm

The adaptive meshing tool is used to maintain a high-quality mesh throughout an analysis even when large deformations occur. Therefore the mesh is allowed to move independently of the material. Adaptive meshing does not change the topology (elements and connectivity) of the mesh. It combines the features of pure Lagrangian analysis (in which the mesh follows the material) and Eulerian analysis (in which the mesh is fixed spatially and the material flows through the mesh). This type of adaptive meshing is often referred to as Arbitrary Lagrangian-Eulerian (ALE) analysis. It is particularly effective to simulate problems with a large amount of non-recoverable deformation like impact or penetration processes. The initial mesh that is optimal for the origin geometry will become more and more unsuitable when the tip penetrates into the soil. The large material deformation leads to severe element distortion and entanglement. Element aspect ratio can also degrade in zones with high strain concentration (e.g. near the tip of the penetrometer). Both factors can lead to a loss of accuracy, a reduction of the size of the stable time increment or to a termination of the calculation.

The following figure (Fig. 10) illustrates the effectiveness of the adaptive mesh procedure. It shows two calculations at an intermediate stage, one using the adaptive mesh tool (left), the other one not (right). You can see the heavy distortion and entanglement of the elements near the cone on the right picture, whereas using the adaptive mesh tool all elements keep their ideal shape throughout the whole calculation.

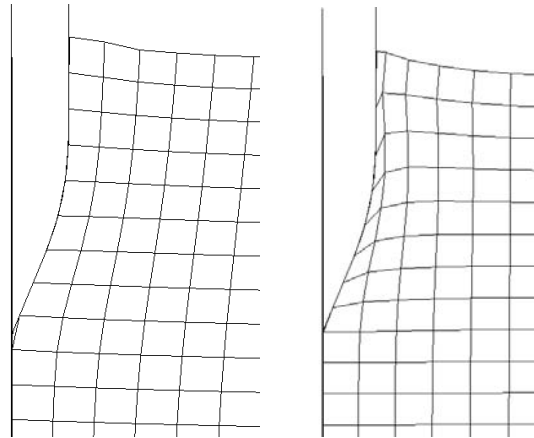


Fig. 10: deformed mesh with (left) and without (right) the adaptive mesh algorithm

4.3 Results

The results presented within this chapter correspond to a calculation with the following parameters:

cone diameter	18 mm
tip shape:	45°
density ρ :	1,55 g/cm ³
Young's Modulus:	20000 kN/m ²
Poisson ratio ν :	0,3
friction angle β :	40°
dilation angle ψ :	2°

In Fig. 11 the vertical stresses in the sample after the first calculation step (gravity) are plotted. The stresses increase with depth according to Eq. 7.

$$\sigma_z = \sigma_2 = \gamma \cdot g \cdot z \quad (7)$$

with	ρ	initial dry density [g/cm ³]
	g	gravity [m/s ²]
	z	depth [m]

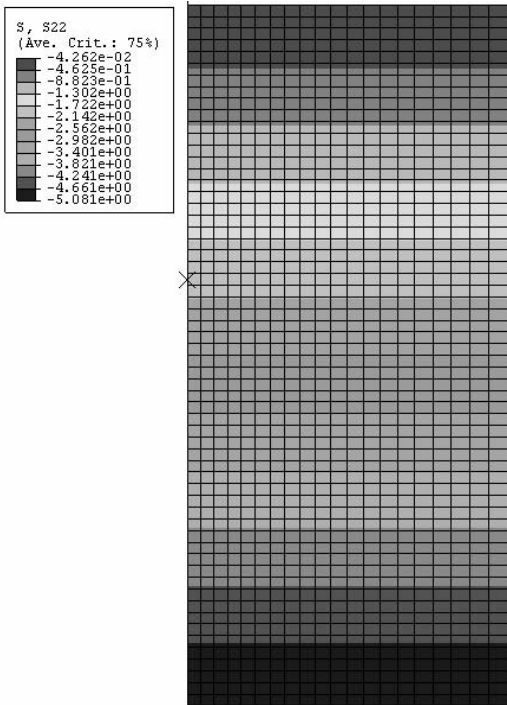


Fig. 11: initial conditions (vertical stress)

Fig. 12 shows the calculation at an intermediate state. The darker regions correspond to nodes where the stress states are in contact with the yield surface. So it can be seen how far the plastic deformations reach into the soil. For this calculation this is about 4 times the radius of the cone.

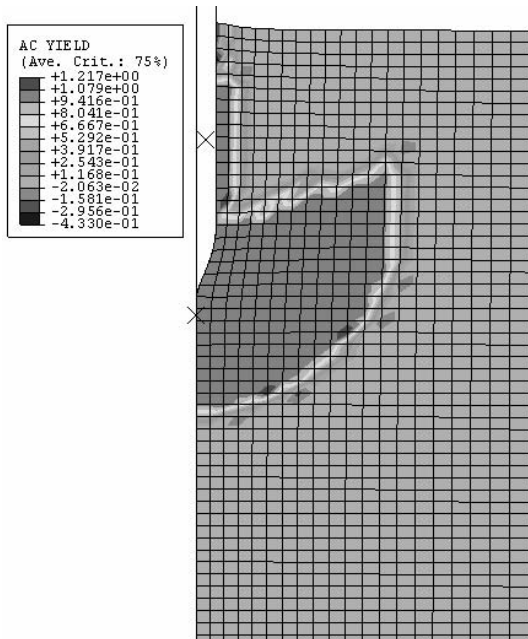


Fig. 12: active yielding points

The compaction of the soil due to the displacements forced by the penetrating tip cause higher stresses beneath and beside the tip. This can be seen by the distribution of the principle stresses which is shown in Fig. 13.

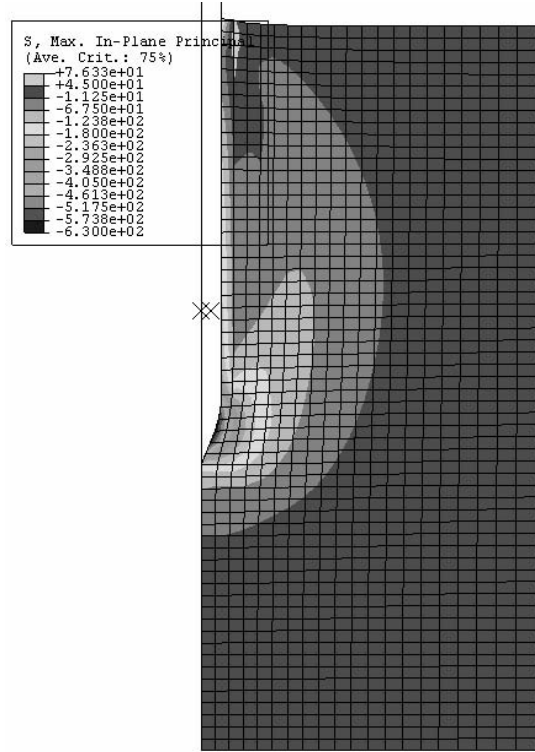


Fig. 13: principal stresses at max. depth

The comparison between the numerical calculation and the laboratory tests can be done with the diagram penetration force vs. depth. The result of the calculation is shown in Fig. 14 and can be compared with Fig. 5 which shows the result of the laboratory test.

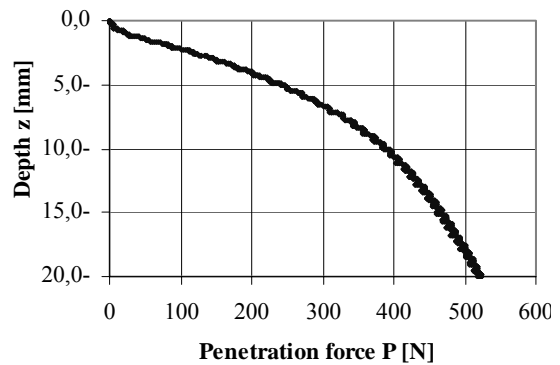


Fig. 14: Penetration force vs. depth

One difference is the initial increase of the penetration force at the first approx. 5 cm which is much higher for the calculation. This is due to the fact that for the real soil the Young's modulus increases with depth and has a very low value especially at the surface. Whereas the dependence of the Young's modulus from the depth is not yet implemented in the soil model used.

Apart from this initial region the inclination of the two curves as well as the maximum force reached are well comparable.

5. CONCLUSION

The numerical modelling of the penetration process of probes into granular materials with the finite element method is a challenging problem due to the limitations of the continuum formulation. So it makes great demands on the software and the model used. In comparison with the laboratory tests the results of the presented model show good correlations. The model has proved an adequate accuracy to recalculate laboratory tests and, after a full calibration with the existing tests, to perform parametric studies. So the influence of parameters and conditions which cannot be changed in the laboratory can be determined.

6. REFERENCES

1. Kömle, N.I.; Ball,A.J.; Kargl,G.; Stöcker,J; Thiel,M.; Jolly,H.S; Dziruni,M.; Zarnecki,J.C., *Using the anchoring device of a comet lander to determine surface mechanical properties*, Planet. Space Sci., 45, No. 12, 1515-1538, 1997.
2. Kargl, G., Macher, W., Kömle, N.I., Thiel, M., Rohe, C., Ball, A.J., *Accelerometry measurements using the Rosetta Lander's anchoring harpoon: experimental set-up, data reduction and signal analysis*, Planetary and Space Science, 49, No. 425-435, 2001.
3. Christensen, P.R.; Moore, H.L., *The Martian Surface Layers*, Mars, Kieffer et al. (Eds.), University of Arizona Press, 686-729, 1992.
4. Lunne, T., Robertson, P.K., Powell, J.J.M., *Cone Penetration Testing in Geotechnical Practice*, Blackie Academic and Professional, London (312 pages), 1997.
5. Grabe, J., König, F., *Zur aushubbedingten Reduktion des Drucksondierwiderstandes*, Bautechnik, 7, No. 569-577, 2004
6. Huang, W., Sheng, D., Sloan, S.W., Yu, H.S., *Finite Element Analysis of Cone Penetration in Cohesionless Soil*, Research Report No. 222.01.2002, University of Newcastle, Australia, 2002.
7. Hibbitt, Karlsson, Sorensen, *ABAQUS Analysis User's Manual*, Version 6.5, 2004.